JOC The Journal of Organic Chemistry

Article

pubs.acs.org/joc

Computational and DNMR Analysis of the Conformational Isomers and Stereodynamics of Secondary 2,2′-Bisanilides

Andrea Mazzanti,*[,†] Michel Chiarucci,[†] Luca Prati,[†] Keith W. Bentley,[‡] and Christian Wolf*[,‡]

[†]Department of Industrial Chemistry "Toso Montanari", University of Bologna, Viale Risorgimento 4, I-40136 Bologna, Italy

[‡]Department of Chemistry, Georgetown University, Washington, DC 20057, United States

Supporting Information

ABSTRACT: The conformational preference of 2,2′-bisanilides was investigated by variable-temperature NMR spectroscopy, NMR titration and diffusion experiments, IR spectroscopy, computational analysis, and X-ray crystallography. The formation of a conformation having the two amide moieties linked by an intramolecular hydrogen bond was detected at low temperatures. The interconversion kinetics of the two conformational species of bisanilide **2** were determined by NMR line shape analysis. The formation of a supramolecule linked by intermolecular hydrogen bonds was ruled out by means of DMSO titration, DOSY experiments, and steric considerations.

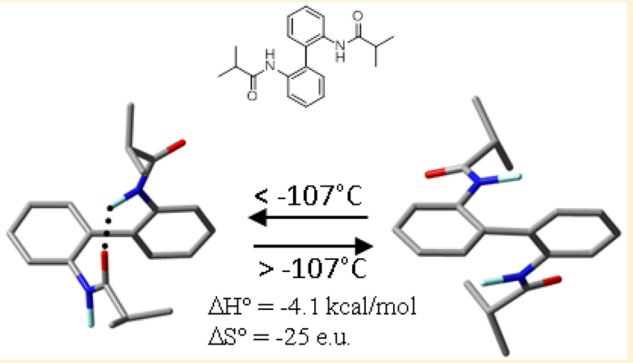

INTRODUCTION

The structural diversity and unique dynamic stereochemistry of amides continues to attract widespread attention among medicinal and synthetic chemists.[1] The control of steric interactions and stereoelectronic forces that affect the conformational bias of tertiary amide units in peptoids, e.g., non-natural peptide analogues consisting of N-substituted glycine monomers, is essential for manipulating backbone folding and chiral amplification processes of these and other important peptidomimetics.[2] The *E*/*Z*-isomerism and atropisomerism of tertiary benzamides, naphthamides and other structural analogues showing restricted rotation about the aryl-carbonyl bond have been studied by Clayden, Walsh, and others and are well-known to play important roles in asymmetric synthesis, medicinal chemistry, and chiral amplification processes.[3] For similar reasons, Curran and others have investigated the relative stability and interconversion of rotational conformers and *E*/*Z* -isomers of tertiary anilides in great detail.[4] Despite the remarkable utility of secondary anilides as auxiliary groups in asymmetric synthesis,[5] the dynamic stereochemistry of this structural motif remains largely unexplored.[6]

We recently reported that 2,2′-binaphthalene-1,1′-diol diisobutyrate **1** shows a complex stereodynamic behavior due to hindered rotation about the central naphthyl−naphthyl axis and the two aryl−ester bonds.[7] The latter process results in the formation of three conformational diastereoisomers when the rotation about the stereogenic aryl−aryl axis is blocked. At the outset of our investigation, we speculated that the secondary bisanilide **2** and analogues thereof would have similar stereochemical properties (Figure 1).

RESULTS AND DISCUSSION

When initial NMR analysis of 1,1′-biphenyl-2,2′-diamine diisobutyramide, **2**, was performed between 25 °C and −99 °C using CD_2Cl_2 as solvent the expected line shape evolution for the isopropyl signals was not observed. Although the two anisochronous doublets corresponding to the diastereotopic methyls of the isopropyl group clearly indicate that the rotation about the aryl−aryl bond is slow on the NMR time scale at ambient temperature, we did not detect any conformational diastereoisomer due to hindered rotation about the *N*-aryl bond under cryogenic conditions. The multiplicity of the two methyl signals and of the isopropyl CH septet remains unchanged upon cooling to −78 °C. When the sample was cooled to −99 °C a series of new signals arose in both the aliphatic and aromatic regions of the spectrum. In particular, at least 4 new broad peaks emerged between 4 and 10 ppm (Figure S1 in the Supporting Information (SI)). Because it seemed unlikely that this could be attributed to dynamic exchange of conformational isomers, further investigations were carried out to elucidate the nature of this unexpected behavior.

Additional ^{1}H NMR spectra of **2** were then recorded at lower temperature using a mixture of $CDFCl_2$:CDF_2Cl (5:1 v/v) as solvent (Figure 2). Again, at −107 °C a new set of signals between 4 and 10.5 ppm emerged at once from the baseline without any heavy broadening effect on the other NMR signals already present. No significant changes were observed when the sample was further cooled to −139 °C. In spite of extensive overlap of the broad signals, a close inspection of the aliphatic

Received: October 7, 2015
Published: December 10, 2015

DOI: 10.1021/acs.joc.5b02330
J. Org. Chem. 2016, 81, 89−99

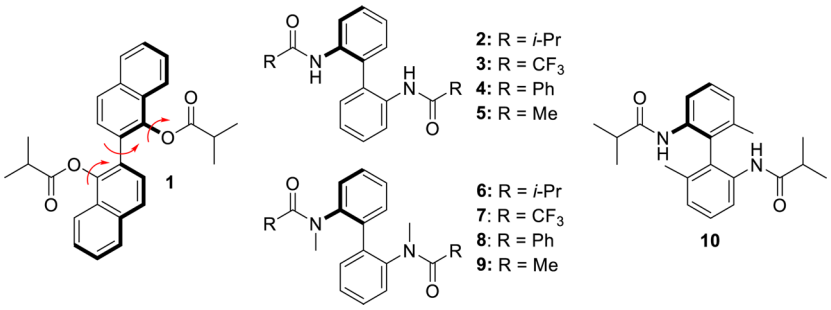

Figure 1. Comparison of the structure of 2,2′-binaphthalene-1,1′-diol diisobutyrate, **1**, and structural analogues **2**−**10** investigated herein.

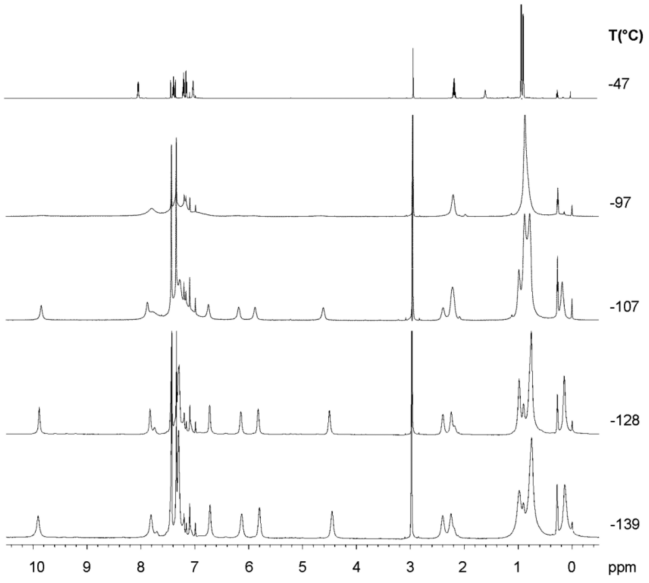

Figure 2. Temperature dependence of the ^{1}H NMR spectra of **2** (600 MHz in $CDFCl_2/CDF_2Cl$ 5/1 v/v).

region in the ^{1}H NMR spectrum suggested the presence of two species in approximately 4:1 ratio, the major one displaying four CH_3 and two CH signals and the minor showing two CH_3 and one CH signals (Figure S2 in the SI).

Given the low polarity of the Freon mixture, a new set of spectra was acquired in a 50 mM sample of **2** in $CDFCl_2/CDF_2Cl$ containing 50 μL of CD_3OD (about 3 equiv).[8] When the sample was cooled, no significant variations were observed in the NMR spectra until −128 °C, and at −139 °C the same set of new signals appeared between 5 and 10 ppm (Figure S3 in the SI). However, the second set of signals emerged at lower temperature with respect to the sample without CD_3OD. This suggests that the presence of methanol alters the equilibrium between the distinct species of **2** which ultimately leads to the appearance of the second set of signals. The variable-temperature NMR experiments were also repeated in a more dilute solution (25 mM) with or without addition of CD_3OD, but appreciable variations were not observed. When a very diluted sample (2 mM) was cooled to −140 °C, the second set of signals was still present, albeit with a lower intensity (see Figure S4 in the SI). In this case, however, any trace of moisture present in the solvents can alter the equilibria at a great extent (see NMR Titration Experiments section). A line shape simulation of the more concentrated sample was performed in the −97 to −107 °C temperature range by considering two identical rate constants that exchange the single signal of the C_2 conformation into the two signals of the C_1 conformation (see Figure S5 in the SI).[9] Assuming reversible first-order reaction kinetics, we obtained three rate constants (70, 35, and 15 s^{-1}) corresponding to an activation energy of 8.6 ± 0.2 kcal/mol. Although the temperature range investigated was small, there is no evidence of a noticeable $\Delta S^{\ddagger}$. On the contrary, the relative ratio between the two conformations changes with the temperature and linear regression analysis was performed to determine $\Delta H°$ as −4.1 kcal/mol and $\Delta S°$ as −25 cal/(mol K) for the interconversion of the C_2 conformation to the C_1 species (see Figure S5 in the SI).[10]

The same experimental NMR results discussed above for **2** were obtained with the secondary amides bearing the trifluoromethyl, phenyl, and methyl groups (**3**−**5**, see Figure S6 in SI). On lowering the temperature, a new set of signals emerged with chemicals shift pattern very similar to that observed for the isopropyl analogue **2**. However, the ratio between the two species varied within the series of **2**−**5** with the methyl derivative **5** showing the smallest amount of the asymmetric species.

Single crystals of compound **2** suitable for X-ray diffraction were grown from slow evaporation of a chloroform solution, and crystals of **5** were obtained from an acetonitrile solution. In both cases, the solid-state structure shows the presence of an intramolecular hydrogen bond with global C_1 symmetry (Figure 3) as well as an intermolecular hydrogen-bond with the neighboring molecules forming an infinite chain (Figure S7 in SI).

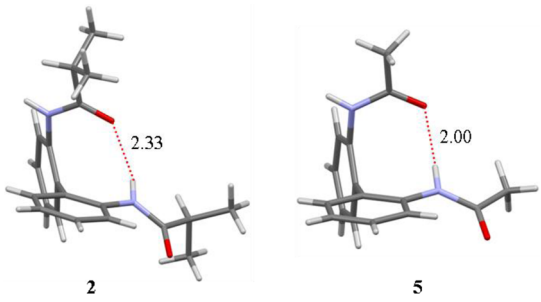

Figure 3. X-ray structures of bisanilides **2** and **5**; distances in Å.

In contrast, the X-ray structure of bisanilide **3** (crystals obtained from chloroform, Figure 4) showed the existence of two different C_2 conformations with an intermolecular hydrogen bond connecting the CO with the NH of the neighbor molecules (see Figure S7 in SI). In the two conformations, the disposition of the amide moiety is largely different. In one conformation, the H−N−C2−C1 dihedral angle is 31.4°, while it is −121.7° in the other. This different disposition allows for the formation of intermolecular hydrogen

DOI: 10.1021/acs.joc.5b02330
J. Org. Chem. 2016, 81, 89−99

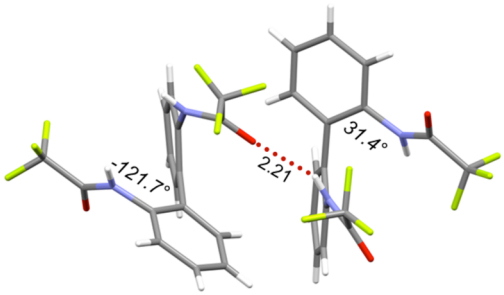

Figure 4. X-ray structure of bisanilide **3**. The numbers in italics measure the H−N−C2−C1 dihedral angles of the two different conformations.

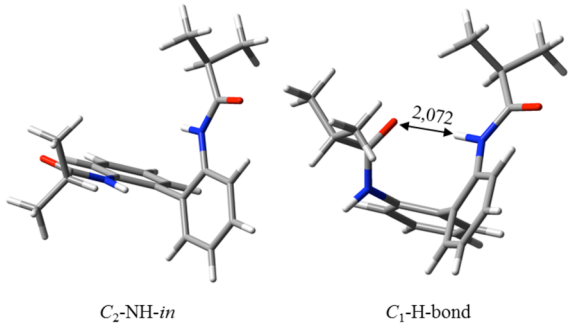

Figure 5. Two most stable conformations of compound **2** calculated at the B3LYP/6-31G(d) level; distances in Å.

bonds only. It is evident that the conformational preference in the solid state is driven by minute energy differences, and crystal packing forces can play a decisive role.

Two scenarios should be considered to rationalize the experimental data obtained in solution. First, the formation of an intramolecular hydrogen bond (as in the X-ray structures of **2** and **5**) results in molecular asymmetry which affords two methine signals and four methyl signals in the case of **2** as well as eight signals for the aromatic hydrogens. Based on this hypothesis, the predominant set of signals observed at low temperature for compounds **2**−**5** should be assigned to the C_1 conformation found in the solid state. Second, the appearance of new signals at low temperatures could be a result of the formation of a dimeric structure, as previously reported for a series of biphenyl carbinols.[11] The presence of a dimer of **2** in solution could explain the main set of signals observed at −128 °C (two isopropyl CH signals with the same intensity), and the coexistence of monomeric **2** could afford the second set of signals (one CH and two methyls). Compounds **2**−**5** contain two identical amide moieties that can act both as hydrogen-bond donor and acceptor, and the differentiation between the two scenarios is not straightforward. As a first consideration, we point out that the X-ray structures of **2**, **3**, and **5** do not show dimers in the solid state, while in the case of biphenyl carbinols the dimeric structures observed in solution were experimentally observed also in the solid state. To obtain more information about the present case, we designed a set of theoretical and experimental analyses.

Theoretical Analysis. A theoretical investigation of compound **2** using B3LYP/6-31G(d) suggested that in the most stable conformation, hereafter named **C_2-NH-*in***, the amide moieties lie in the plane of the phenyl rings, yielding global C_2 symmetry. The carbonyl groups point toward the aromatic hydrogen adjacent to the amide unit (H3) and do not undergo hydrogen bonding with the NH belonging to the other ring (Figure 5). A conformation close to that observed in the crystal (hereafter named **C_1-H-bond**) was validated as a local minimum about 2 kcal/mol higher in energy. The same situation occurs for compound **5**, where the **C_2-NH-*in*** is calculated to be more stable than **C_1-H-bond** by 2.8 kcal/mol and by 12.0 kcal with respect to the other C_2 conformation (**C_2-NH-*out*** hereafter).

However, when a different theoretical level such as M06-2X/6-31G(d,p) was employed for optimization, the two conformations have essentially the same energy (see Figure S8 in SI), and at the ωB97XD/6-31G(d,p) level, the **C_1-H-bond** conformation is not a minimum of energy (optimization starting from the M06-2X optimized geometry reverted to **C_2-NH-*in*** geometry) as summarized in Table 1. These striking results underscore the complexity of the stereodynamic behavior of **2**.

At this point, X-ray analysis of **2** revealed that the most stable conformation in the solid state features C_1 symmetry and an intramolecular hydrogen bond, whereas the conformation **C_2-NH-*in*** emerged as the most or exclusively populated species according to B3LYP/6-31G(d) and ωB97XD/6-31G(d) computations, while M06-2X calculations suggest that the **C_1-H-bond** and the **C_2-NH-*in*** conformations should have similar stabilities.

If we consider the formation of dimers, two kinds of structures should be discussed. Due to the stereogenic aryl−aryl axis, the dimer can be built using two molecules with the same axial chirality ("homodimer") or from two molecules with opposite chirality ("heterodimer"). In the first case the whole symmetry can be C_2 or C_1, whereas in the second case the symmetry can be C_i or C_s. Two stable dimeric structures (frequency calculation displayed no imaginary values) were obtained for both cases (Figure 6), with very similar energies. At the B3LYP/6-31G(d) level, the heterodimer is more stable by 0.5 kcal/mol (as $\Delta H°$), while the M06-2X/6-31G(d) level computation favors the heterodimer by 2.7 kcal/mol (as $\Delta H°$). The heterodimer features C_i symmetry, and the homodimer is C_2 symmetric. Both structures are in agreement with the NMR analysis showing four signals for the isopropyl methyl groups. Due to the different local environment, there are two different isopropyl groups for each molecule, each one related to another by the inversion center or by the rotation axis. Taking into account the intrinsic diastereotopicity of the isopropyl methyls, a total of four signals for the methyl and two signals for the methine groups is expected, as was observed experimentally.

The individual conformation of the two molecules of the heterodimer resembles that of the **C_2-NH-*in***, the aryl−aryl torsion angle being 113°. Two NH moieties are nearly coplanar with the aryl rings, whereas the remaining two are slightly out-of-plane to accommodate a better geometry for the hydrogen bond (skew angle = 21°). The homodimer is composed of two molecules with similar conformation and torsion angle (114°). The dimerization energy was evaluated using the counterpoise correction suggested by Bernardi and Boys[12] (see Table 2) and was found to be 6.8 kcal/mol for the heterodimer and 5.0 kcal/mol for the homodimer (21.3 and 18.3 kcal/mol at the counterpoise-corrected M06-2X/6-31G(d) level). Within the dimeric structure, the two NMR signals at 4.5 and 9.9 ppm could be correlated to the two pairs of NHs, with the signal at 9.9 ppm corresponding to the pair involved in the intermolecular hydrogen bond,[13] and that at 4.5 ppm assigned

DOI: 10.1021/acs.joc.5b02330
J. Org. Chem. 2016, 81, 89−99

Table 1. Computational Data for the Two Most Stable Conformations of 2[a]

conformation	method	energy (au)	ΔE (kcal/mol)	$H°$ (au)	$\Delta H°$ (kcal/mol)
C_2-NH-*in*	B3LYP	−1036.596083	**0.00**	−1036.164819	**0.00**
C_1-H-bond	B3LYP	−1036.591816	2.68	−1036.161215	2.26
C_2-NH-*in*	M06-2X	−1036.185695	**0.00**	−1035.751855	0.17
C_1-H-bond	M06-2X	−1036.185473	0.13	−1035.752128	**0.00**
C_2-NH-*in*	ωB97XD	−1036.281224	0.08	−1035.845280	0.58
C_1-H-bond	ωB97XD	−1036.281361[b]	**0.00**	−1035.846213	**0.00**

[a]This structure converged to C_2 symmetry with a biphenyl torsion angle of 66°. [b]The same 6-31G(d) basis set was employed in the calculations.

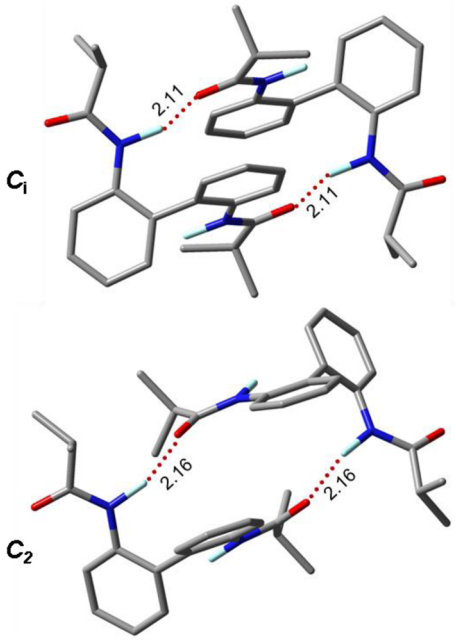

Figure 6. Optimized structures of the dimers of **2**; distances in Å. Optimization at the B3LYP/6-31G(d) level. Except for the NH, all the hydrogens were removed for clarity.

to the remaining pair of free NH groups that are shielded by the phenyl ring currents. Although we could not obtain experimental support for the assignment of these two signals (HSQC is unfeasible at −140 °C), the averaged chemical shift of these signals (7.2 ppm) is in very good agreement with the higher temperature shift of the NH units (7.0 ppm at −50 °C)

The dimerization energies for **3**−**5** were also calculated at two different level of theory taking into account the intrinsic BSSE error by the counterpoise correction (Table 2). The energy gain for dimerization (E_{dim} in Table 1) favors the formation of the heterodimer in all cases. This is most probably due to the smaller distortion required to the two monomers to get a favorable interaction between the NH and C═O in the heterodimer. On the contrary, the trend of the relative energies calculated for the dimers (as global optimization of the supramolecule) is not constant.

The homodimers of compounds **3** and **4** (CF_3 and phenyl) were calculated to be *more* stable than the heterodimers at both levels of theory. This effect is probably due to the larger BSSE error evaluated for the homodimer and to the greater distortion of the two monomers to reach a geometry suitable for the formation of the dimer. Albeit the large dimerization energy calculated with M06-2X could suggest that the hypothesis of a dimerization process should be favored over that of the formation of an intramolecular hydrogen bond. The inconsistent trend observed for compounds **2**−**5** and the huge difference in the dimerization energies determined by the two methods did not allow for a reliable interpretation.

As an additional way to rationalize the experimental NMR results, we calculated the chemical shifts of the two monomeric conformations of **2** and of the two dimers (Table 3).

Table 3. Summary of Calculated Chemical Shifts for Compound 2[a]

	NH	NH′	H-3	H-3′
C_1-H-bond	8.1	6.5	9.0	7.4
C_2-NH-*in*	6.7	6.7	9.5	9.5
heterodimer	8.7	7.5	9.5	9.0
homodimer	8.2	7.5	9.0	8.5

[a]Calculations at the GIAO-B3LYP/6-311++G(2d,p)//B3LYP/6-31G(d) level. Reported chemical shift are related to that of TMS calculated at the same level of theory.

Calculations were run at the GIAO-B3LYP/6-311++G-(2d,p)//B3LYP/6-31G(d) level of theory. In the case of the **C_1-H-bond** conformation the chemical shift difference between the two NH units is larger than in the case of the dimers. In absolute terms, the chemical shift of the free NH in the **C_1-H-bond** conformation is more shielded than that of the free NH in both dimers. If the chemical shift of the hydrogen *ortho* to the carbonyl (H-3) is considered, it is worth noting that the conformations of the dimers have all carbonyl groups arranged

Table 2. Summary of Dimers Energies and Dimerization Energies for 2−5[a]

	B3LYP/6-31G(d)				M06-2X/6-31G(d)			
	heterodimer		homodimer		heterodimer		homodimer	
	E	E_{dim}	E	E_{dim}	E	E_{dim}	E	E_{dim}
2	**0.00**	−6.8	0.50	−5.0	**0.00**	−21.3	2.67	−18.3
3	0.75	−5.5	**0.00**	−0.6	0.54	−17.2	**0.00**	−13.1
4	5.55	−4.3	**0.00**	−1.6	0.31	−24.0	**0.00**	−17.7
5	**0.00**	−8.6	2.03	−6.4	**0.00**	−18.0	1.16	−17.8

[a]Dimerization energies E_{dim} were calculated with counterpoise correction (all energies are in kcal/mol).

DOI: 10.1021/acs.joc.5b02330
J. Org. Chem. 2016, 81, 89−99

almost coplanar to the aryl rings, and the proximity of the carbonyl group should move the H-3 signal downfield. Calculations support this hypothesis and suggest a chemical shift difference of 0.5 ppm. On the contrary, the calculated chemical shift difference for the **C_1-H-bond** conformation is much larger (1.6 ppm). The observed upfield shift of the H-3 signal on lowering the temperature is therefore more consistent with the formation of an intramolecular hydrogen bond.

IR Spectroscopy. In a different attempt to elucidate the structure of the main species we resorted to IR spectroscopy. Because of the much faster time scale compared to NMR spectroscopy, a high-resolution IR spectrum of compound **2** dissolved in $CDCl_3$ was acquired with the aim to detect, either in the NH- or in the CO-stretching region, separated signals for the two conformations observed by NMR at low-temperature (Figure 7). Interestingly, the NH region of the spectrum

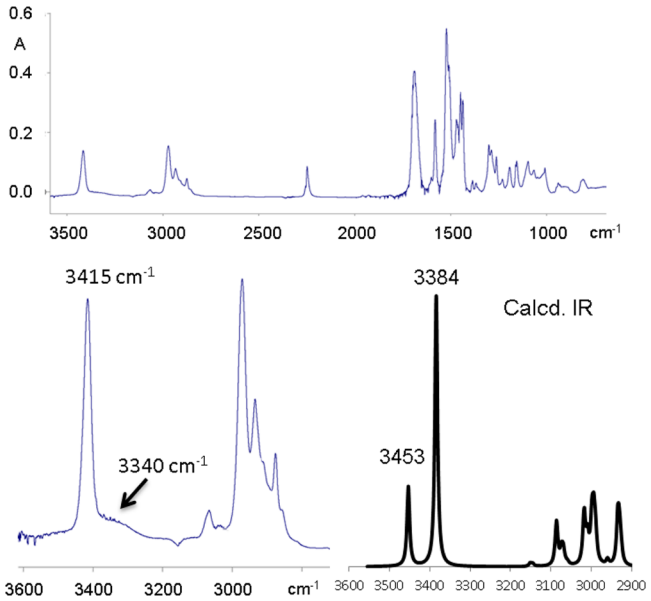

Figure 7. Top: IR spectra of **2** in $CDCl_3$ solution after solvent subtraction. Bottom left: IR excerpt of the N−H stretching region of the spectrum. Bottom right: Calculated IR spectrum of **2** for the same spectral region at the B3LYP/6-31G(d) level.

exhibits a sharp band at 3415 cm^{-1} accompanied by a broad band at lower frequency (3340 cm^{-1}). Although the shape of the bands in this spectral region may be strongly affected by the presence of water or by the concentration of the sample, similar results have been attributed to an equilibrium between amides not involved in hydrogen bonding (sharp band above 3400 cm^{-1}) and amides exhibiting hydrogen bonding (broad band at 3300−3350 cm^{-1}).[13]

The IR spectrum of the **C_1-H-Bond** conformation of **2** as well of the two dimers was calculated at the B3LYP/6-31G(d) level of theory, and the calculated frequency was scaled by 0.9614.[14] For the monomer, two strong IR absorbances were calculated for the NH stretching. The lower frequency absorption (3384 cm^{-1}) was calculated for the stretching of the NH moiety involved in the intramolecular hydrogen bonding, whereas a higher frequency (3453 cm^{-1}) was obtained for the two free NH units. This is in agreement with the experimental spectrum. Since the calculations correspond to isolated molecules in the gas phase, any line-broadening contributions from solvent interactions are not taken into account. However, the same kind of IR behavior can be rationalized with the presence of two intermolecular hydrogen bonds (broad band) and of two free NH groups (sharp band) in the dimeric structures (see Figure S9 in the SI for the simulations).

NMR Titration Experiments. To obtain additional data, we monitored changes in the δ-shift occurring when **2** was titrated with DMSO-d_6. It is known that hydrogen bonding results in proton deshielding, thus the addition of DMSO or another strong hydrogen-bond acceptor should result in a downfield shift for an NH proton that is available for hydrogen bonding with a polar solute. On the other hand, if a competing intramolecular hydrogen bond already exists, the downfield shift should be limited.[15] When aliquots of DMSO-d_6 were added to a $CDCl_3$ solution of **2** two signals were strongly shifted: the NH proton moved downfield by more than 1 ppm, and the H3 proton (located adjacent to the amide group in the phenyl ring) was shifted upfield by 0.4 ppm (Figure 8). All other signals were not affected. These results could be rationalized by a competition of DMSO with the exchanging hydrogen bonds, yielding a conformational change. The upfield shift of the aromatic proton in position 3 (H3) suggests that, upon solvent complexation, the amide carbonyl moves out of the plane of the aryl ring and thus away from H3.

In an attempt to model this behavior, DFT calculations were carried out by considering the interactions with one and two explicit molecules of the hydrogen-bond acceptor DMSO (Figure 9). Full optimization was performed for the substrate-solute adducts, and the stabilization energies due to the interactions were determined as the difference between the counterpoise corrected[12] energy of the complex and the sum of the energies of **C_2-NH-*in*** and one or two isolated solute molecules. All the calculations confirmed that the **C_1-H-bond** conformation is stabilized by hydrogen bonding with a solute molecule with respect to the free **C_2-NH-*in*** species, with stabilization energy higher than 8 kcal/mol. When two DMSO molecules were considered during optimization, the conformation of the bisanilide displays C_2 symmetry with the amides moved out of the plane by 38° and a stabilization energy of 16.4 kcal/mol (as counterpoise corrected value).

The interaction between DMSO and **2** and the modification of the amide disposition can explain the shifts observed during titration. This seems to support the hypothesis that a strong intramolecular hydrogen bond is responsible for the set of signals observed at low temperature.

To rationalize the experimental spectroscopic and crystallographic data obtained with **2**, we therefore suggest the model shown in Figure 10. The **C_2-NH-*in*** conformation is stabilized by conjugation of the amide with the phenyl ring, while the **C_1-H-Bond**, found to be the most stable species in the solid state, is stabilized by intramolecular hydrogen bonding. At room temperature the two species are in fast exchange and contribute to an averaged NMR spectrum. On lowering the temperature, the exchange rate decreases, and the signals belonging to both conformations can be distinguished, which explains the appearance of the new signals under cryogenic conditions. The fact that the peaks emerge at once from the baseline rather than from a dynamic exchange of the existing signals can be explained by a large variation in the population ratio of the two conformers as a function of temperature. If the two conformations have similar enthalpies, entropic factors (and therefore temperature) may become important and greatly affect the relative population. Because hydrogen bonding plays

DOI: 10.1021/acs.joc.5b02330
J. Org. Chem. 2016, 81, 89−99

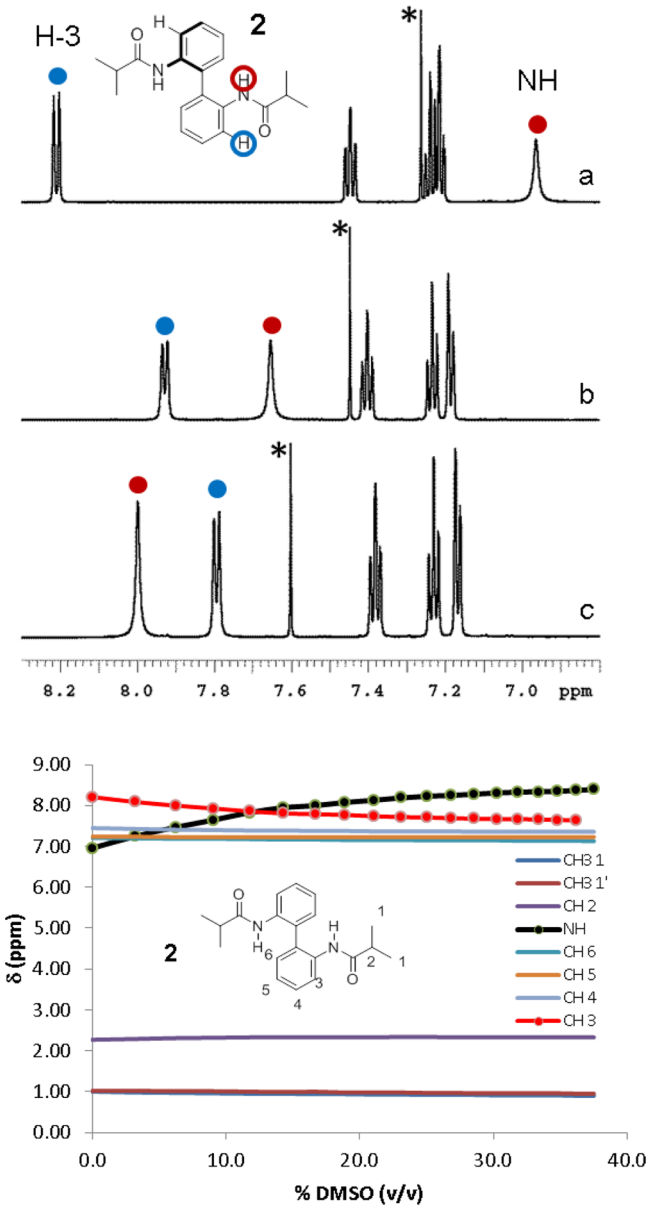

Figure 8. Top: ^{1}H NMR aromatic region of bisanilide **2** in $CDCl_3$ (600 MHz, 25 °C) obtained by DMSO titration. The sample was prepared by dissolving 7.7 mg (23.8 μmol) of **2** in 0.6 mL of $CDCl_3$. (a) control spectrum; (b) 60 μL of DMSO added; and (c) 120 μL of DMSO added. The asterisks mark the residual signal of $CDCl_3$. Bottom: changes in the chemical shift of the ^{1}H NMR signals of **2** during DMSO titration.

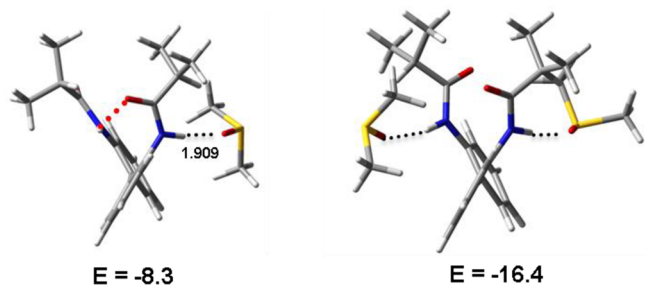

Figure 9. Structures and stabilization energies of **2**−solute complexes optimized at the B3LYP/6-31G(d) level. The reference energy was that of **C_2-NH-in** plus one or two isolated molecules of DMSO. Distances in Å, and energies in kcal/mol.

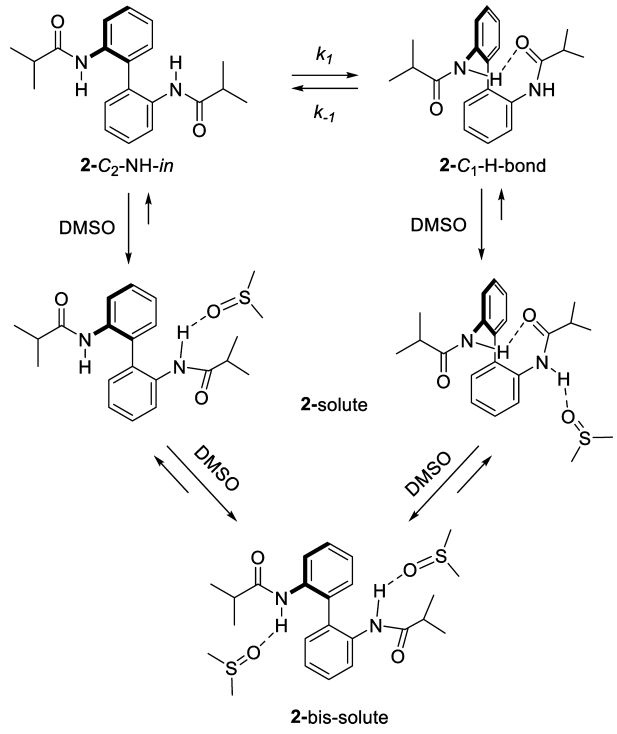

Figure 10. Proposed model to explain the dynamic behavior of **2** in solution.

an important role here, the presence of hydrogen-bond acceptors can affect the relative stability of the two conformations, which is evident from the titration experiments with DMSO. When a strong acceptor is added it can interact with the free NH of the **C_1-H-Bond** species or with one of the two free NH groups of the **C_2-NH-*in*** conformer. As the amount of the hydrogen-bond acceptor is increased, the solute can afford a second hydrogen bond which ultimately leads to a bis-solute. In this case both carbonyls are displaced out of the phenyl plane, thus explaining the large upfield shift experienced by H-3.

Within the series of compounds **2**−**5**, the change in the ratio of the two species observed at low temperature can be rationalized by the different interactions between the carbonyl residues and the solvent additive. Hydrogen-bonding interactions with DMSO may be more sterically hindered with compound **2** bearing relatively large isopropyl groups, while this interaction with the acetyl derivative **5** is more accessible. With regard to dimerization, similar considerations should play a role. In this case, the smaller the aliphatic residue next to the carbonyl function the larger should be the dimer proportion, as experimentally observed in the case of biphenyl bis-carbinols.[11] The opposite experimental trend found with **2**−**5** could rule out the hypothesis of dimer formation at low temperature and supports the prevalence of a strong intramolecular hydrogen bond.

On the other hand, the formation of any hydrogen bond relies on a delicate balance of conformational geometries that can arrange the amide groups in close proximity without substantially raising the conformational energy. A close inspection of the X-ray structures of compounds **2** and **5** revealed that the aryl−aryl dihedral angles are 109.9° and 95.4°, respectively. We therefore speculated that any interference due

DOI: 10.1021/acs.joc.5b02330
J. Org. Chem. 2016, 81, 89−99

to other conformational constraints could greatly influence the intramolecular hydrogen-bonding interaction. To explore this matter we acquired variable-temperature NMR spectra of the tetra-ortho-substituted bisanilide **10**, i.e., the atropisomeric analogue of compound **2**. This secondary amide can be prepared starting from enantiopure (*M*)-6,6′-dimethyl-2,2′-diaminobiphenyl as well as from the racemic precursor. The considerable steric repulsion between the ortho-substituents forces the dihedral angle to approximately 90° and significantly decreases the conformational flexibility compared to compounds **2**−**5**. The increased rigidity poses more constraints to any interaction requiring a modification of the aryl−aryl bite angle. Moreover, enantiopure **10** can be used to rule out the feasibility of formation of a heterodimer.

We found that the NMR spectra of a $CDFCl_2$ sample of enantiopure (*M*)-**10** were completely different from those observed for compounds **2**−**5**. The low-temperature NMR analysis of (*M*)-**10** did not reveal any additional signals down to −140 °C. In fact, we observed only a large downfield shift of the amide proton, while the neighboring hydrogen H3 moved upfield from 7.9 to 7.3 ppm, crossing with the NH signal (Figure 11). The very same behavior was obtained when a

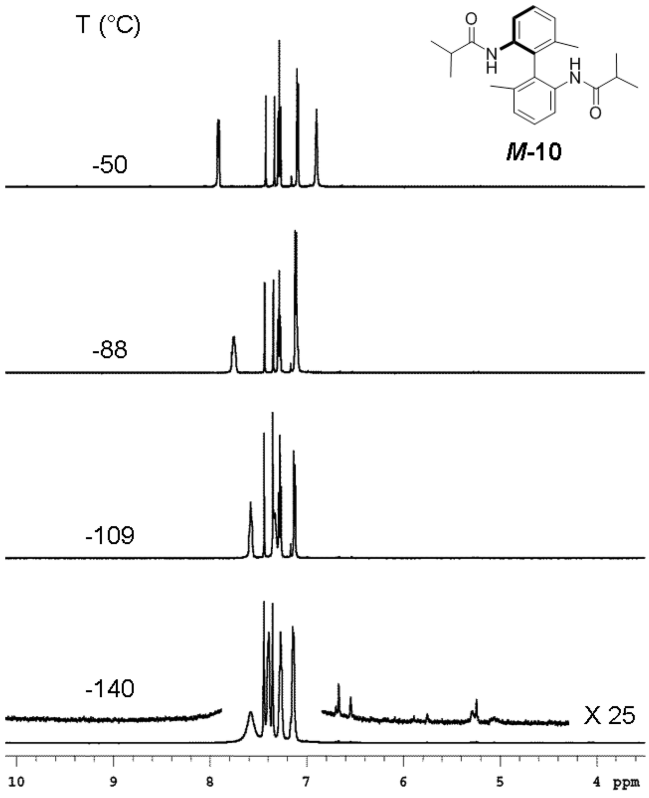

Figure 11. Low-temperature spectra of (*M*)-**10**, showing the absence of additional signals at −140 °C. Spectra of racemic **10** are reported in Figure S10 in SI.

sample of racemic **10** was used (see Figure S10 in the SI). No additional signals were detected down to −140 °C, and the same chemical shifting of the NH and H-3 signals occurred. However, when compared to compound **2**, the downfield shift of the NH signal is less pronounced, while the upfield shift of H-3 remains comparable.

The dimerization energies for the hetero- and homodimer of compound **10** were calculated and found to be 5.9 and 5.8 kcal/mol at the counterpoise-corrected B3LYP/6-31G(d) level (20.9 and 17.8 kcal/mol at the M062X/6-31G(d) level). Thus, calculations predict for the dimers of **10** the same stabilization as for compound **2**, while the experimental NMR of **10** at low temperature does not show the second set of signals. This suggests again that the experimental results are more reliable than the computational analysis and that dimerization does not take place. On the other hand, the absence of the second set of signals can be explained by considering the same conformational change observed for **2**. In the case of compound **10**, the constraints imposed by the fixed aryl−aryl angle impede the accommodation of a geometry necessary for effective intramolecular hydrogen bonding. Because the intramolecular hydrogen bond is diminished, the barrier for the interconversion falls below the limit of the dynamic NMR technique. Accordingly, the spectrum observed at −140 °C can still be attributed to fast dynamic exchange within the **C_1-H-bond** conformation. Unfortunately, spectra at lower temperature could not be obtained due to crystallization of the compound.

NMR Diffusion Experiments. DOSY spectra were acquired for compounds **2** and **10** in $C_2D_2Cl_4$ that is in a solvent similar to $CDCl_3$ but with increased viscosity. The NMR spectra were collected with the BPP-STE sequence using an array of gradient strength from 1 to 62 G/cm and a diffusion delay of 50 ms. The residual signal of the solvent was used as internal standard to compare different spectra. Since the derived hydrodynamic radius is related to the diffusion coefficient, the ratios of the diffusion coefficient of each compound vs that of the solvent correspond to the relative ratios of the hydrodynamic radii between solute and solvent. As the hydrodynamic radius of the solvent is the same, we can directly compare the radii of the solutes. The derived hydrodynamic radius for **2**, racemic **10** and for enantiopure (*M*)-**10** were very similar (SI). For the three compounds, the ratio with the solvent radius is 2.30:1 (±0.05) and was almost invariant when more concentrated samples (10 times) were used. Since dimerization should be favored at increasing concentration, these results further point to the importance of intramolecular hydrogen bonding.

Comparison with Tertiary Amides. To further verify whether interactions involving the NH moiety are exclusively responsible for the observed stereochemical behavior of secondary amides, we synthesized the tertiary amides **6**−**9**. As a representative example, the ^{1}H NMR spectrum of the tertiary bisanilide **9** recorded in $CDCl_3$ at room temperature shows a number of broad signals in both the N-Me and CH_3CO regions corresponding to at least three equilibrating species (Figure S11 in SI). While in secondary amides only the Z amide conformer is usually populated, in tertiary amides both conformations are present. The three sets of signals were therefore assigned to the three possible diastereoisomers generated by hindered rotation around the two N−CO bonds. Two isomers with the same conformation of the partial double bond of the amide moiety have global C_2 symmetry and can be referred to as *ZZ*-**9** and *EE*-**9**. The third conformation with global C_1 symmetry displays opposite orientation of the two amides and is named *EZ*-**9**.

Single crystals of compound **9** were obtained by evaporation of an acetonitrile solution, and the X-ray structure confirmed the different conformational preference (Figure 12). In the solid state, a C_2 conformation is present, with both amides having *E* geometry. The dihedral angle C1−C2−N−CO is −125.1°, while the aryl−aryl torsion angle was determined as 70.0°.

DOI: 10.1021/acs.joc.5b02330
J. Org. Chem. 2016, 81, 89−99

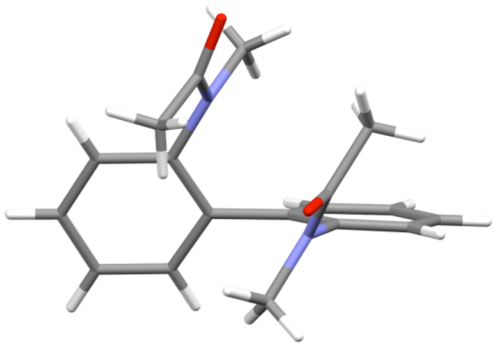

Figure 12. X-ray structure of compound **9**.

When a $CDFCl_2/CDF_2Cl$ (5/1 v/v) NMR sample of **9** was analyzed at low temperatures, certain signals further broadened and eventually split into a large number of peaks (Figure S12 in the SI), following the classical evolution of a conformational exchange. The trend resembles what was observed for the binaphthyl ester **1**, and the new signals in the lowest temperature spectrum have been ascribed to a number of diastereoisomers formed when the rotation about the two N-aryl bonds is frozen. From a theoretical point of view, up to 9 different stereoisomers can be formed and up to 14 singlets in the N-Me and 14 in the CH_3CO region should appear. For each diastereoisomer generated by the hindered rotation about the N−CO bond (i.e., *ZZ, EE, EZ*), three possible orientations of the two amides can be considered depending on the reciprocal orientation of the two N-Me (or C═O) groups (Figure S13 in the SI). The *ZZ* and *EE* N−CO conformers yield two C_2 and one C_1 conformations each, thus a total of eight signals are expected, while the *EZ* yields three C_1-symmetric conformers, corresponding to additional six lines. Unfortunately, partial signal overlapping and the presence of several conformers scarcely populated made it difficult to establish with full accuracy the number of species present. Thus, the stereochemical analysis of the tertiary anilides **6**−**9** confirmed that there is dynamic exchange between several conformational isomers due the perpendicular disposition of the amide moiety with respect to the aryl rings. Although the system is complicated by the presence of tertiary amide *E*/*Z* isomers (contrary to the secondary bisanilides where only the *Z* isomer is present), from a stereodynamic point of view compounds **6**−**9** behaves like the binaphthyl ester **1.**

CONCLUSIONS

We have investigated the conformational preference of a series of 2,2′-bisanilides using variable-temperature NMR spectroscopy, NMR titration and diffusion experiments, IR spectroscopy, computational analysis, and crystallography. In addition to the generally expected **C_2-NH-in** species, the formation of a **C_1-H bond** conformation having the two amide moieties linked by an intramolecular hydrogen bond was detected at low temperatures. The formation of a dimeric species in solution was ruled out by means of steric considerations, DMSO titration, and DOSY experiments and supported by chemical shift calculations and comparison with the behavior of known biphenyl carbinols. The interconversion kinetics of the two conformational species of bisanilide **2** were determined by NMR line shape analysis, and the temperature dependence of the conformational ratio gave unique insights into enthalpic and entropic terms that affect the equilibrium which favors formation of an intramolecular hydrogen bond below −107 °C.

EXPERIMENTAL SECTION

All reagents and solvents were commercially available and used without further purification. Reactions were carried out under inert atmosphere and anhydrous conditions. Flash chromatography was performed on silica gel, particle size 40−63 μm. NMR spectra were obtained at 600 MHz (^{1}H NMR) and 150 MHz (^{13}C NMR) using the residual signals of the solvents (CD_3CN or $CDCl_3$) as chemical shift reference.[16] 2,2′-Diaminobiphenyl and (*M*)-6,6′-dimethyl-2,2′-diaminobiphenyl were commercially available. *N*,*N*′-Dimethyl-2,2′-diaminobiphenyl was prepared according to the literature.[17]

1,1′-Biphenyl-2,2′-diamine Diisobutyramide, 2. 2,2′-Diaminobiphenyl (50 mg, 0.27 mmol, 1 equiv) and NEt_3 (94 μL, 0.68 mmol, 2.5 equiv) were dissolved in 5 mL of dichloromethane and cooled to 0 °C. Isobutyryl chloride (68 μL, 0.65 mmol, 2.4 equiv) was added, and the mixture was slowly warmed to room temperature and stirred for 2 h. The reaction was quenched with water and extracted with dichloromethane. The combined organic layers were dried over $MgSO_4$ and concentrated in vacuo. Purification by flash chromatography on silica gel (CH_2Cl_2:EtOAc 85:15) afforded 85 mg (0.26 mmol, 95%) of a white solid. Mp 137−139 °C. Crystal suitable for X-ray diffraction were obtained by slow evaporation of a $CHCl_3$ solution. ^{1}H NMR (600 MHz, CD_3CN, +25 °C): δ = 0.91 (d, J = 6.8 Hz, 6H), 0.96 (d, J = 6.8 Hz, 6H), 2.28 (septet, J = 6.8 Hz, 2H), 7.18 (dd, J = 7.6 Hz, 1.7 Hz, 2H), 7.27 (dd, J = 7.6 Hz, 8.1 Hz, 2H), 7.42 (dd, J = 8.1 Hz, 7.6 Hz, 2H), 7.63 (s, 2H), 7.77 (d, J = 8.1 Hz, 2H). ^{13}C NMR (150 MHz, CD_3CN, +25 °C): δ = 19.4 ($2CH_3$), 19.5 ($2CH_3$), 36.3 (2CH), 125.8 (2CH), 126.2 (2CH), 129.4 (2CH), 131.4 (2CH), 133.6 (2Cq), 136.9 (2Cq), 176.8 (2CO). Anal. calcd for $C_{20}H_{24}N_2O_2$: C, 74.05; H, 7.46; N, 8.63. Found: C, 74.01; H, 7.73; N, 8.59.

1,1′-Biphenyl-2,2′-diamine Bis(trifluoromethylacetamide) 3.[18] 2,2′-Diaminobiphenyl (60 mg, 0.33 mmol, 1 equiv) and NEt_3 (95 μL, 0.68 mmol, 2 equiv) were dissolved in 5 mL of dichloromethane and cooled to 0 °C. Trifluoroacetic anhydride (114 μL, 0.82 mmol, 2.5 equiv) was added, and the mixture was slowly warmed to room temperature and stirred for 4 h. The reaction was quenched with water and extracted with dichloromethane. The combined organic layers were dried over $MgSO_4$ and concentrated in vacuo. Purification by flash chromatography on silica gel (CH_2Cl_2:EtOAc 85:15) afforded 92 mg (0.24 mmol, 75%) of a brown solid. Mp 163−165 °C. Crystal suitable for X-ray diffraction were obtained by slow evaporation of a $CHCl_3$ solution. ^{1}H NMR (600 MHz, CD_3CN, +25 °C): δ = 7.30 (d, J = 7.6 Hz, 2H), 7.45 (dd, J = 7.6 Hz, 7.9 Hz, 2H), 7.54 (dd, J = 7.9 Hz, 7.6 Hz, 2H), 7.69 (d, J = 7.9 Hz, 2H), 8.71 (bs, 2H). ^{13}C NMR (150 MHz, CD_3CN, +25 °C): δ = 116.8 (q, J_{CF} = 288 Hz, $2CF_3$), 126.7 (2CH), 128.5 (2CH), 130.3 (2CH), 131.7 (2CH), 133.5 (2Cq), 134.5 (2Cq), 156.6 (2CO). ^{19}F NMR (376 MHz, $CDCl_3$): δ = −76.1.

1,1′-Biphenyl-2,2′-diamine Dibenzamide, 4.[19] 2,2′-Diaminobiphenyl (80 mg, 0.43 mmol, 1 equiv) and NEt_3 (150 μL, 1.09 mmol, 2.5 equiv) were dissolved in 5 mL of dichloromethane and cooled to 0 °C. Benzoyl chloride (106 μL, 0.91 mmol, 2.1 equiv) was added, and the mixture was slowly warmed to room temperature and stirred for 2 h. The reaction was quenched with water and extracted with dichloromethane. The combined organic layers were dried over $MgSO_4$ and concentrated in vacuo. Purification by flash chromatography on silica gel (CH_2Cl_2:EtOAc 85:15) afforded 130 mg (0.33 mmol, 75%) of a white solid. Mp 182−185 °C. ^{1}H NMR (600 MHz, CD_3CN, +25 °C): δ = 7.28−7.33 (m, 4H), 7.41−7.48 (m, 6H), 7.53 (m, 2H), 7.66 (m, 4H), 7.81 (d, J = 7.4 Hz, 2H), 8.58 (s, 2H). ^{13}C NMR (150 MHz, CD_3CN, +25 °C): δ = 126.6 (2CH), 126.8 (2CH), 127.9 (4CH), 129.5 (4CH), 129.6 (2CH), 131.4 (2CH), 132.7 (2CH), 135.1 (2Cq), 135.3 (2Cq), 136.8 (2Cq), 167.1 (2CO).

1,1′-Biphenyl-2,2′-diamine Acetamide, 5. 2,2′-Diaminobiphenyl (612 mg, 0.33 mmol, 1 equiv) and 4-aminopyridine (40 mg, 0.033 mmol, 1 equiv) were dissolved in 4 mL (40 mmol, 12 equiv) of acetic anhydride. The dark-orange mixture was stirred for 1 h at 75 °C. The

DOI: 10.1021/acs.joc.5b02330
J. Org. Chem. 2016, 81, 89−99

reaction was quenched with 20 mL of HCl (0.2M). The solution was diluted with 20 mL of dichloromethane, and the organic phase was separated. The aqueous phase was extracted with DCM (3 × 15 mL), and the combined organic layers were washed with a saturated aqueous solution of $NaHCO_3$ (20 mL) and brine (20 mL), then dried over Na_2SO_4. Purification by flash chromatography on silica gel (hexane:ethyl acetate 80:20) afforded 680 mg (2.54 mmol, 76%) of a white solid. Mp 152−156 °C. Crystal suitable for X-ray diffraction were obtained by slow evaporation of a acetonitrile solution.^{1}H NMR (600 MHz, CD_3CN, +25 °C): δ = 1.84 (s, 6H), 7.21 (dd, J = 7.6 Hz, 1.6 Hz, 2H), 7.27 (dd, J = 7.6 Hz, 7.6 Hz, 2H), 7.42 (dd, J = 7.6 Hz, 8.1 Hz, 2H), 7.62 (s, 2H), 7.83 (d, J = 8.1 Hz, 2H). ^{13}C NMR (150 MHz, CD_3CN, +25 °C): δ = 23.7 ($2CH_3$), 125.5 (2CH), 126.1 (2CH), 129.4 (2CH), 131.8 (2CH), 132.5 (2Cq), 136.9 (2Cq), 170.0 (2CO). Anal. calcd for $C_{16}H_{16}N_2O_2$: C, 71.62; H, 6.01; N, 10.44. Found: C, 71.36; H, 5.73; N, 10.32.

***N,N′*-(6,6′-Dimethyl-[1,1′-biphenyl]-2,2′-diyl)bis(2-methylpropanamide) 10 and (*M*)-*N,N′*-(6,6′-Dimethyl-[1,1′-biphenyl]-2,2′-diyl)bis(2-methylpropanamide) (*M*)-10.** In an oven-dried two-necked round-bottomed flask, 6,6′-dimethyl-2,2′-diaminobiphenyl[20] or (*M*)-6,6′-dimethyl-2,2′-diaminobiphenyl (0.24 mmol, 1 equiv) was dissolved in 2 mL of anhydrous dichloromethane, and the solution was cooled at 0 °C. Triethylamine (1.44 mmol, 6 equiv) and isobutyryl chloride (0.96 mmol, 4 equiv) were added in sequence. The solution was stirred at room temperature until complete consumption of the starting material (TLC, 3 h). The reaction mixture was diluted with dichloromethane (10 mL) and quenched with 1 M HCl (5 mL) at 0 °C. The organic layer was washed with brine (10 mL) and saturated aqueous solution of $NaHCO_3$ (2 × 5 mL). The organic phase was dried over Na_2SO_4, and the solvent was removed under reduced pressure to afford the product as a pale-brown amorphous solid in 82% yield (69 mg, 0.19 mmol). ^{1}H NMR (600 MHz, $CDCl_3$, +25 °C) δ = 0.92 (d, J = 6.6 Hz, 6H), 0.97 (d, J = 6.6 Hz, 6H), 1.97 (s, 6H), 2.23 (septet, J = 6.6 Hz, 2H), 6.98 (bs, 2H), 7.15 (d, J = 7.8 Hz, 2H), 7.34 (dd, J = 7.8 Hz, 7.9 Hz, 2H), 8.03 (d, J = 7.8 Hz, 2H). ^{13}C NMR (150 MHz, $CDCl_3$, +25 °C) δ = 19.0 ($2CH_3$), 19.1 ($2CH_3$), 19.5 ($2CH_3$), 36.2 (2CH), 120.3 (2CH), 126.4 (2CH), 127.1 (2Cq), 129.0 (2CH), 135.7 (2Cq), 137.0 (2Cq), 175.4 (2CO). GC-MS (m/z): 352 (25) $[M]^+$, 309 (5) $[M\text{-iPr}]^+$, 282 (25), 239 (25), 212(20), 195 (100), 180 (15), 71(15). Anal. calcd for $C_{22}H_{28}N_2O_2$: C, 74.97; H, 8.01; N, 7.95. Found: C, 74.78; H, 8.39; N, 7.85.

***N,N′*-([1,1′-Biphenyl]-2,2′-diyl)bis(*N*-methyl-2-dimethylpropanamide) 6.** In an oven-dried round balloon purged with nitrogen, a solution of *N,N′*-dimethyl-2,2′-diaminobiphenyl (0.47 mmol, 1 equiv) in dichloromethane (4 mL) was cooled at 0 °C, and 5.7 mmol (12 equiv) of TEA was added. Isobutyryl chloride (3.8 mmol, 8 equiv) was added dropwise, and the reaction mixture was stirred and allowed to return to the room temperature in 3 h. The reaction was quenched with HCl (1M), and the phases were separated. The aqueous phase was extracted with DCM (3 × 10 mL). The combined organic layers were washed with a saturated aqueous solution of $NaHCO_3$ (20 mL) and brine (20 mL) and dried over Na_2SO_4. The solvent was removed under reduced pressure, and the desired product was obtained as a white solid (113 mg, 0.32 mmol) by semipreparative HPLC in 70% yield. Column: LUNA-C18 (250 × 21.20 mm), MeCN/H_2O 80/20, 20 mL/min, λ 254 nm, t_R: 4.72 min. Mp 152−154 °C. ^{1}H NMR (600 MHz, $CDCl_3$, +25 °C): δ = 0.80 (bs, 1H), 1.4 (d, J = 6.7 Hz, 1H), 1.08 (d, J = 6.7 Hz, 4H), 1.14 (d, J = 6.7 Hz, 4H), 1.17−1.27 (bs, 2H). 2.25 (bs, 0.3H) 2.39 (sept, J = 6.7 Hz, 0.3H), 2.59 (sept, J = 6.7 Hz, 1.4H), 2.79−2.87 (bs, 4H), 2.95 (bs, 0.7H), 3.07 (bs, 1H), 3.37 (bs, 0.3H), 7.24 (bs, 1H), 7.29 (bm, 2.6H), 7.33 (bm, 0.6H), 7.39 (bm, 2.2H), 7.43(bm, 1.4H), 7.47 (bs, 0.2H). ^{13}C NMR (150 MHz, $CDCl_3$, +25 °C): δ = 18.8, 19.0, 19.6, 20.3, 20.7 (b), 30.4, 31.4, 31.6 (b), 35.6 (b), 128.1, 128.2, 128.7, 129.2$_7$, 129.3$_4$, 129.4, 129.5, 130.9, 131.2, 134.0, 134.7, 141.4, 141.8, 177.5, 177.8 (b). Anal. calcd for $C_{22}H_{28}N_2O_2$: C, 74.97; H, 8.01; N, 7.95. Found: C, 74.57; H, 8.43; N, 7.83.

***N,N′*-([1,1′-Biphenyl]-2,2′-diyl)bis(2,2,2-trifluoro-*N*-methylacetamide) 7.** A solution of 1.0 mL of trifluoroacetic anhydride was cooled to 0 °C, and 0.1 mmol (1 equiv) of *N,N′*-dimethyl-[1,1′-biphenyl]-2,2′-diamine was added. The solution was stirred for 1 h at room temperature and then diluted with ethyl acetate and quenched with HCl (1 M, 10 mL). The organic layer was washed with brine (10 mL), and a saturated aqueous solution of $NaHCO_3$ (10 mL). The organic phase was dried over Na_2SO_4, and the solvent was evaporated under reduced pressure to afford a sticky solid. A sample was purified by preparative HPLC on the LUNA-C18 phase (250 × 21.20 mm), MeCN/H_2O 70/30, 20 mL/min, λ 254 nm, t_R: 9.14 min. The HPLC purification gave 32 mg (0.08 mmol,80%) of a sticky solid. ^{1}H NMR (600 MHz, $CDCl_3$, +25 °C) δ = 2.80 (s, 1.2H), 2.86 (bs, 0.6H), 2.95−3.07 (bm, 1.8H), 3.15 (bs, 0.9H), 3.54−3.66 (bs, 1.5H), 7.24−7.52 (bm, 8H). ^{19}F NMR (564 MHz, $CDCl_3$, +25 °C) δ = −66.1, −66.2, −67.2, −70.2, −70.3, −70.6, −70.8. ^{13}C NMR (150 MHz, $CDCl_3$, +25 °C) δ = 37.1, 37.4 (b), 39.7 (b), 116.4 (q, J = 291.7 Hz, CF3), 127.2 (b), 128.4, 128.9, 129.1 (b), 129.7, 129.8, 130.0 (b), 130.5, 131.0, 133.4 (b), 134.0 (b), 134.7, 138.2, 140.0 (b), 140.7 (b), 156.1(b), 157.4, 157.6, 157.8, 158.1. HRMS (ESI-QTOF) anal. calcd for $C_{18}H_{15}F_6N_2O_2$: 405.1032. Found: 405.1038. Anal. calcd for $C_{18}H_{14}F_6N_2O_2$: C, 53.47; H, 3.49; N, 6.93. Found: C, 53.12; H, 3.85; N, 6.69.

General Procedure for the Preparation of Tertiary Amides 8 and 9.

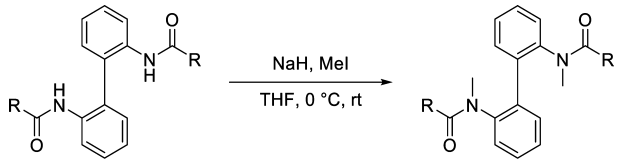

In an oven-dried Schlenk tube under nitrogen atmosphere 0.2 mmol (1 equiv) of amide was dissolved in 1 mL of anhydrous THF, and the solution was cooled at 0 °C. NaH (60% dispersion in mineral oil, 0.5 mmol, 2.5 equiv) was added, and the reaction mixture was stirred for 15 min at ambient temperature, then MeI (0.6 mmol, 3 equiv) was added at 0 °C. The reaction mixture was stirred at ambient temperature until complete consumption of the starting material (TLC, 2−6 h) and then quenched with a saturated solution of NH_4Cl (5 mL). The aqueous phase was extracted with ethyl acetate (3 × 5 mL), and the combined organic layers were washed with brine (10 mL) and then dried over Na_2SO_4. The solvent was removed under reduced pressure to afford the desired product which was used as is or purified by semipreparative HPLC for the variable-temperature NMR analysis.

***N,N′*-([1,1′-Biphenyl]-2,2′-diyl)bis(*N*-methylbenzamide) 8.** Using **4** in the protocol described above, we obtained 56 mg (67% yield) of a white solid. Mp 157−159 °C. ^{1}H NMR (600 MHz, $CDCl_3$, +25 °C) δ = 1.98 (s, 0.4H), 3.07 (bs, 2.9H), 3.56 (s, 2.7H), 5.95 (bs, 1.3H), 6.85 (bdd, J = 6.0 Hz, J = 6.0 Hz, 0.8H), 7.03−7.20 (bm, 4.2H), 7.20−7.69 (bm, 9.1H). ^{13}C NMR (150 MHz, $CDCl_3$, +25 °C) δ = 37.7, 125.6, 126.5 (b), 127.1, 127.2, 127.6, 128.2, 128.4, 128.7, 129.3, 129.5, 129.8, 130.9 (b), 132.5, 135.0, 135.2, 135.3, 136.0 (b), 141.2, 142.0, 168.9, 169.7, 172.0 (b). Anal. calcd for $C_{28}H_{24}N_2O_2$: C, 79.98; H, 5.75; N, 6.66. Found: C, 79.53; H, 5.65; N, 6.66

***N,N′*-([1,1′-Biphenyl]-2,2′-diyl)-bis(*N*-methylacetamide) 9.** Using **5** in the protocol described above, we obtained 38 mg (63% yield) of a white solid. Mp 175−177 °C. Crystals suitable for X-ray analysis were obtained by slow evaporation of a $CDCl_3$ solution. ^{1}H NMR (600 MHz, $CDCl_3$, +25 °C) δ = 1.85 (s, 1.2H), 2.01 (bs, 4.1H), 2.16 (bs, 0.7H), 2.77 (bs, 4.1H), 2.87 (bs, 0.5H), 2.96 (s, 1.5H), 3.37 (bs, 0.7H), 7.24 (bd, 1.9H), 7.27 (d, J = 7.2 Hz, 1.4H), 7.31 (bd, 0.6H), 7.37 (bm, 0.5H), 7.41−7.44 (bm, 3.5H). ^{13}C NMR (150 MHz, $CDCl_3$, +25 °C) δ = 22.0, 22.5, 22.6, 22.7, 35.4, 36.6, 127.9, 128.1, 128.2, 129.1, 129.2, 129.3, 131.2, 132.4, 135.0, 136.1, 141.8, 142.1, 170.7, 170.9, 171.0. Anal. calcd for $C_{18}H_{20}N_2O_2$: C, 72.95; H, 6.80; N, 9.45. Found: C, 72.57; H, 6.49; N, 9.85.

Variable-Temperature NMR. Variable-temperature NMR spectra were recorded with a spectrometer operating at a field of 14.4 T (600 MHz for ^{1}H and 150.8 MHz for ^{13}C NMR). Low-temperature ^{1}H NMR spectra were acquired without spinning using a 5 mm dual direct

DOI: 10.1021/acs.joc.5b02330
J. Org. Chem. 2016, 81, 89−99

probe with a 9000 Hz sweep width, 3.0 μs (30° tip angle) pulse width, 3 s acquisition time, and 1 s delay time. A shifted sine bell weighing function equal to the acquisition time (i.e., 3 s) was applied prior to the Fourier transformation. Usually 32−64 scans were collected. Low-temperature 150.8 MHz ^{13}C NMR spectra were acquired without spinning and under proton decoupling conditions with a 38,000 Hz sweep width, 4.5 μs (45° tip angle) pulse width, 1 s acquisition time, and 1 s delay time. A line broadening function of 1−2 Hz was applied before the Fourier transformation. Usually 256−1024 scans were collected. Temperature calibrations were performed using a digital thermometer and a Cu/Ni thermocouple placed in an NMR tube filled with isopentane or 1,1,2,2-tetrachloroethane (for the low and high temperature range, respectively). The conditions were kept as equal as possible with all subsequent work. The uncertainty in temperature measurements can be estimated as ±1 °C. Line shape simulations were performed using a PC version of the QCPE DNMR6 program.[21] Electronic superimposition of the original spectrum and of the simulated one enabled the determination of the most reliable rate constant. The rate constants, thus obtained at various temperatures, afforded the free energy of activation, $\Delta G^{\ddagger}$, by applying the Eyring equation. Within the experimental uncertainty due to the exact temperature determination, the activation energies were found to be invariant, thus implying a small activation entropy $\Delta S^{\ddagger}$.[22]

Calculations. The conformational searches were preliminarily carried out by means of the molecular mechanics force field (MMFF) using the Monte Carlo methods. The most stable conformers thus identified were subsequently calculated by DFT computations that were performed by the Gaussian 09 rev D.01[23] series program using standard optimization parameters. The calculations employed B3LYP,[24] ωB97XD,[25] M06-2X,[26] and the 6-31G(d) basis sets. Harmonic vibrational frequencies were calculated for all the stationary points. As revealed by the frequency analysis, imaginary frequencies were absent in all ground states, whereas one imaginary frequency was associated with each transition state. Visual inspection of the corresponding normal mode[27] validated the identification of the transition states.

■ ASSOCIATED CONTENT

Supporting Information

The Supporting Information is available free of charge on the ACS Publications website at DOI: 10.1021/acs.joc.5b02330.

NMR spectra, crystallographic analysis and computational details (PDF)

Crystallographic data (CIF)

Crystallographic data (CIF)

Crystallographic data (CIF)

Crystallographic data (CIF)

■ AUTHOR INFORMATION

Corresponding Authors

*andrea.mazzanti@unibo.it

*cw27@georgetown.edu

Notes

The authors declare no competing financial interest.

■ ACKNOWLEDGMENTS

This material is partially based upon work supported by the NSF under CHE-1464547. A.M. Thanks the University of Bologna (RFO funds 2014 and FARB project "Catalytic transformation of biomass-derived materials into high added-value chemicals"). ALCHEMY Fine Chemicals & Research (Bologna, www.alchemy.it) is gratefully acknowledged for a generous gift of chemicals.

■ REFERENCES

(1) (a) Lanyon-Hogg, T.; Ritzefeld, M.; Masumoto, N.; Magee, A. I.; Rzepa, H. S.; Tate, E. W. *J. Org. Chem.* **2015**, *80*, 4370−4377. (b) Sandoval-Lira, J.; Fuentes, L.; Quintero, L.; Hopfl, H.; Hernandez-Perez, J. M.; Teran, J. L.; Sartillo-Piscil, F. *J. Org. Chem.* **2015**, *80*, 4481−4490.

(2) (a) Gorske, B. C.; Bastian, B. L.; Geske, G. D.; Blackwell, H. E. *J. Am. Chem. Soc.* **2007**, *129*, 8928−8929. (b) Sui, Q.; Borchardt, D.; Rabenstein, D. L. *J. Am. Chem. Soc.* **2007**, *129*, 12042−12048. (c) Gorske, B. C.; Stringer, J. R.; Bastian, B. L.; Fowler, S. A.; Blackwell, H. E. *J. Am. Chem. Soc.* **2009**, *131*, 16555−16567. (d) Paul, B.; Butterfoss, G. L.; Boswell, M. G.; Renfrew, P. D.; Yeung, F. G.; Shah, N. H.; Wolf, C.; Bonneau, R.; Kirshenbaum, K. *J. Am. Chem. Soc.* **2011**, *133*, 10910−10919. (e) Caumes, C.; Roy, O.; Faure, S.; Taillefumer, C. *J. Am. Chem. Soc.* **2012**, *134*, 9553−9556. (f) Paul, B.; Butterfoss, G. L.; Boswell, M. G.; Huang, M. L.; Bonneau, R.; Wolf, C.; Kirshenbaum, K. *Org. Lett.* **2012**, *14*, 926−929. (g) Laursen, J. S.; Engel-Andreasen, J.; Fristrup, P.; Harris, P.; Olsen, C. A. *J. Am. Chem. Soc.* **2013**, *135*, 2835−2844. (h) Byrne, L.; Sol, J.; Boddaert, T.; Marcelli, T.; Adams, R. W.; Morris, G. A.; Clayden, J. *Angew. Chem., Int. Ed.* **2014**, *53*, 151−155.

(3) Selected examples: (a) Adams, R.; Gordon, J. R. *J. Am. Chem. Soc.* **1950**, *72*, 2454−2457. (b) Reeves, L. W.; Shaddick, R. C.; Shaw, K. N. *Can. J. Chem.* **1971**, *49*, 3683−3691. (c) Thayumanavan, S.; Lee, S.; Liu, C.; Beak, P. *J. Am. Chem. Soc.* **1994**, *116*, 9755−9756. (d) Gasparrini, F.; Misiti, D.; Pierini, M.; Villani, C. *Tetrahedron: Asymmetry* **1997**, *8*, 2069−2073. (e) Dai, W.-M.; Yeung, K. K. Y.; Liu, J.-T.; Zhang, Y.; Williams, I. D. *Org. Lett.* **2002**, *4*, 1615−1618. (f) Rios, R.; Jimeno, C.; Carroll, P. J.; Walsh, P. J. *J. Am. Chem. Soc.* **2002**, *124*, 10272−10273. (g) Chan, V.; Kim, J. G.; Jimeno, C.; Carroll, P. J.; Walsh, P. J. *Org. Lett.* **2004**, *6*, 2051−2053. (h) Clayden, J.; Lund, A.; Vallverdu, L.; Helliwell, M. *Nature* **2004**, *431*, 966−971. (i) Betson, M. S.; Clayden, J.; Lam, H. K.; Helliwell, M. *Angew. Chem., Int. Ed.* **2005**, *44*, 1241−1244. (j) Clayden, J.; Vallverdu, L.; Helliwell, M. *Chem. Commun.* **2007**, 2357−2359. (k) Clayden, J.; Vallverdu, L.; Clayton, J.; Helliwell, M. *Chem. Commun.* **2008**, 561−563.

(4) Selected examples: (a) Kessler, H.; Rieker, A. *Liebigs Ann. Chem.* **1967**, *708*, 57−68. (b) Shvo, Y.; Taylor, E. C.; Mislow, K.; Raban, M. *J. Am. Chem. Soc.* **1967**, *89*, 4910−4917. (c) Stewart, W. H.; Siddall, T. H., III *Chem. Rev.* **1970**, *70*, 517−551. (d) Oki, M. *Top. Stereochem.* **1984**, *14*, 10−19. (e) Curran, D. P.; Liu, W.; Chen, C. H.-T. *J. Am. Chem. Soc.* **1999**, *121*, 11012−11013. (f) Adler, T.; Bonjoch, J.; Clayden, J.; Font-Bardia, M.; Pickworth, M.; Solans, X.; Sole, D.; Vallverdu, L. *Org. Biomol. Chem.* **2005**, *3*, 3173−3183. (g) Petit, M.; Lapierre, A. J. B.; Curran, D. P. *J. Am. Chem. Soc.* **2005**, *127*, 14994−14995. (h) Bruch, A.; Ambrosius, A.; Fröhlich, R.; Studer, A.; Guthrie, D. B.; Zhang, H.; Curran, D. P. *J. Am. Chem. Soc.* **2010**, *132*, 11452−11454. (i) Tsukagoshi, S.; Ototake, N.; Ohnishi, Y.; Shimizu, M.; Kitagawa, O. *Chem. - Eur. J.* **2013**, *19*, 6845−6850.

(5) (a) Basu, A.; Gallagher, D. J.; Beak, P. *J. Org. Chem.* **1996**, *61*, 5718−5719. (b) Basu, A.; Beak, P. *J. Am. Chem. Soc.* **1996**, *118*, 1575−1576. (c) Thayumanavan, S.; Basu, A.; Beak, P. *J. Am. Chem. Soc.* **1997**, *119*, 8209−8216. (d) Kitagawa, O.; Takahashi, M.; Yoshikawa, M.; Taguchi, T. *J. Am. Chem. Soc.* **2005**, *127*, 3676−3677.

(6) (a) Camilleri, P.; Kirby, A. J.; Lewis, R. J.; Sanders, J. K. M. *J. Chem. Soc., Chem. Commun.* **1988**, 1537−1538. (b) Ilieva, S.; Hadjieva, B.; Galabov, B. *J. Mol. Struct.* **1999**, *508*, 73−80. (c) Gonzalez-de-Castro, A.; Broughton, H.; Martinez-Perez, J. A.; Espinosa, J. F. *J. Org. Chem.* **2015**, *80*, 3914−3920.

(7) Mazzanti, A.; Chiarucci, M.; Bentley, K. W.; Wolf, C. *J. Org. Chem.* **2014**, *79*, 3725−3730.

(8) The exact concentration of the sample slightly changes on lowering the temperature because of the volume contraction of the sample.

(9) This exchange scheme implies that there is no direct exchange between the two signals of the C1 conformer.

(10) A similar dramatic change in the population of interconverting compounds over a small temperature range has been reported:

DOI: 10.1021/acs.joc.5b02330
J. Org. Chem. 2016, 81, 89−99

Lunazzi, L.; Parisi, F.; Macciantelli, D. *J. Chem. Soc., Perkin Trans. 2* **1984**, 1025−1028.
(11) Casarini, D.; Lunazzi, L.; Mancinelli, M.; Mazzanti, A.; Rosini, C. *J. Org. Chem.* **2007**, *72*, 7667−7676.
(12) (a) Boys, S. F.; Bernardi, F. *Mol. Phys.* **1970**, *19*, 553. (b) Simon, S.; Duran, M.; Dannenberg, J. J. *J. Chem. Phys.* **1996**, *105*, 11024−11031.
(13) Gellman, S. H.; Dado, G. P.; Liang, G. B.; Adams, B. R. *J. Am. Chem. Soc.* **1991**, *113*, 1164−1173.
(14) Merrick, J. P.; Moran, D.; Radom, L. *J. Phys. Chem. A* **2007**, *111*, 11683−11700.
(15) Jansma, A.; Zhang, Q.; Li, B.; Ding, Q.; Uno, T.; Bursulaya, B.; Liu, Y.; Furet, P.; Gray, N. S.; Geierstanger, B. H. *J. Med. Chem.* **2007**, *50*, 5875−5877.
(16) Gottlieb, H. E.; Kotlyar, V.; Nudelman, A. *J. Org. Chem.* **1997**, *62*, 7512−7515.
(17) Kano, T.; Tanaka, Y.; Maruoka, V. *Org. Lett.* **2006**, *8*, 2687−2689.
(18) Zhang, S.; Zhang, D.; Liebeskind, L. S. *J. Org. Chem.* **1997**, *62*, 2312−2313.
(19) Ames, D. E.; Opalko, A. *Tetrahedron* **1984**, *40*, 1919−1925.
(20) Gillerspie, K. M.; Sanders, C. J.; Westmoreland, I.; Thickitt, C. P.; Scott, P. *J. Org. Chem.* **2002**, *67*, 3450−3458.
(21) Brown, J. H.; Bushweller, C. H. DNMR6: Calculation of NMR Spectra Subject to the Effects of Chemical Exchange (program 633). *QCPE Bulletin*; Department of Chemistry, Indiana University: Bloomington, Indiana, 1983; Vol. 3, p 103. A PC version of the program is available on request from the authors.
(22) (a) Lunazzi, L.; Mancinelli, M.; Mazzanti, A. *J. Org. Chem.* **2007**, *72*, 5391−5394. (b) Masson, E. *Org. Biomol. Chem.* **2012**, *11*, 2859−2871.
(23) Frisch, M. J.; Trucks, G. W.; Schlegel, H. B.; Scuseria, G. E.; Robb, M. A.; Cheeseman, J. R.; Scalmani, G.; Barone, V.; Mennucci, B.; Petersson, G. A.; Nakatsuji, H.; Caricato, M.; Li, X.; Hratchian, H. P.; Izmaylov, A. F.; Bloino, J.; Zheng, G.; Sonnenberg, J. L.; Hada, M.; Ehara, M.; Toyota, K.; Fukuda, R.; Hasegawa, J.; Ishida, M.; Nakajima, T.; Honda, Y.; Kitao, O.; Nakai, H.; Vreven, T.; Montgomery, J. A., Jr.; Peralta, J. E.; Ogliaro, F.; Bearpark, M.; Heyd, J. J.; Brothers, E.; Kudin, K. N.; Staroverov, V. N.; Kobayashi, R.; Normand, J.; Raghavachari, K.; Rendell, A.; Burant, J. C.; Iyengar, S. S.; Tomasi, J.; Cossi, M.; Rega, N.; Millam, N. J.; Klene, M.; Knox, J. E.; Cross, J. B.; Bakken, V.; Adamo, C.; Jaramillo, J.; Gomperts, R.; Stratmann, R. E.; Yazyev, O.; Austin, A. J.; Cammi, R.; Pomelli, C.; Ochterski, J. W.; Martin, R. L.; Morokuma, K.; Zakrzewski, V. G.; Voth, G. A.; Salvador, P.; Dannenberg, J. J.; Dapprich, S.; Daniels, A. D.; Farkas, O.; Foresman, J. B.; Ortiz, J. V.; Cioslowski, J.; Fox, D. J. *Gaussian 09*, rev D.01; Gaussian, Inc.: Wallingford, CT, 2009.
(24) (a) Lee, C.; Yang, W.; Parr, R. G. *Phys. Rev. B: Condens. Matter Mater. Phys.* **1988**, *37*, 785−789. (b) Becke, A. D. *J. Chem. Phys.* **1993**, *98*, 5648−5652. (c) Stephens, P. J.; Devlin, F.J.; Chabalowski, C. F.; Frisch, M. J. *J. Phys. Chem.* **1994**, *98*, 11623−11627.
(25) Chai, J.-D.; Head-Gordon, M. *Phys. Chem. Chem. Phys.* **2008**, *10*, 6615−6620.
(26) Zhao, Y.; Truhlar, D. G. *Theor. Chem. Acc.* **2008**, *120*, 215−241.
(27) *Package GaussView 5.0.9*; Gaussian Inc.: Wallingford CT, 2009.

DOI: 10.1021/acs.joc.5b02330
J. Org. Chem. 2016, 81, 89−99